Large Current Modulation and Spin-Dependent Tunneling of Vertical Graphene/MoS_2 Heterostructures.

Nojoon Myoung[1], Kyungchul Seo[1, †], Seung Joo Lee[2,], and Gukhyung Ihm[1,]**

[1]Department of Physics, Chungnam National University, Daejoen 305-764, Republic of Korea

[2]Quantum-functional Semiconductor Research Center, Dongguk University, Seoul 100-715, Republic of Korea

[†]Daeduk Campus for BNT Convergence, Paichai University, Daejeon 305-509, Republic of Korea

Supporting Information

1. Quantum-mechanical consideration of tunneling probability through MoS_2 barriers

In order to obtain the tunneling current density, we need to calculate the transmission probability through the barrier as below;

$$T(E) = \exp\left[-\frac{2\sqrt{2m^*}}{\hbar}\int_{-h/2}^{+h/2}\sqrt{U(z)-E}\,dz\right],$$

where m^* is the out-of-plane effective mass of MoS_2 ($0.54m_0$ for electrons and $0.44m_0$ for holes), d is the thickness of the barrier, and $U(z)$ is the potential energy of the barrier as a function of z. This consideration is valid for the direct tunneling regime, i.e., energy of tunneling carriers has to be always less than $U(z)$. Since there is an electric field between top and bottom graphene layers, the tunnel barrier must be a function of z, $U(z) = \Delta_{c,v} + qV_b z/d$, where $\Delta_c \cong 0.5$ eV and $\Delta_v \cong 1.4$ eV are the barrier height for electrons and holes, respectively.

Now, let us discuss effects of the band-movement at the interfaces between the MoS_2 and graphene. In the recent literature[1], tunneling current can be modulated by taking into

account Schottky barriers when the sandwiched MoS_2 layer is doped. In fact, in this study, we consider an undoped MoS_2 as an intrinsic semiconductor. In this case, there is no charge transfer from metal (graphene) to semiconductor (MoS_2), so that we do not need to take into account any band-bending which is a result of the formation of depletion layers. Therefore, we can calculate transmission probability by using the flat band edges that have been proven to be reasonable for hBN by L. Britnell et al[2].

2. Non-linearity of carrier concentration induced by gate voltage

The heterostructure used in this study is consists of two graphene layers and a thin MoS_2 layer, and the graphene layers are doped by applying gate voltage via a back gate electrode separated by an insulating layer as illustrated in Fig. 1 in the main text. Carrier concentration n_{bot} and n_{top} in both bottom and top graphene layers induced by the gate voltage V_g has to satisfy following equations;

$$\epsilon_{MoS_2}\frac{V_{ind}}{h} - \epsilon_{sub}\frac{V_g}{d} = en_{bot},$$
$$\epsilon_{MoS_2}\frac{V_{ind}}{h} = -en_{top},$$
$$-\epsilon_{sub}\frac{V_g}{d} = ep,$$

where ϵ_{MoS_2} and ϵ_{sub} are dielectric constant of MoS_2 and substrate, and h and d are the thickness of MoS_2 layer and substrate, respectively. V_{ind} in these equations is a finite voltage difference between two graphene layers as below

$$eV_{ind} = \sqrt{\pi}\hbar v_F\left(\sqrt{n_{top}} - \sqrt{n_{bot}}\right).$$

Combining above equations, one can obtain an equation regarding to n_{top};

$$\frac{e^2 n_{top} h}{\epsilon_{MoS_2}} + \sqrt{\pi}\hbar v_F\left(\sqrt{n_{top}} + \sqrt{n_{top} + \frac{\epsilon_{sub}V_g}{ed}}\right) = 0,$$

and n_{top} is calculated numerically. Similarly, n_{bot} is also calculated in the same manner. Here, we put n_{top} and n_{top} positive values in the case of n-doped graphene layers, but they can be negative in the case of p-doped grahene layers when the gate voltage is inversely applied. The calculated carrier concentration in the top and the bottom graphene layers is exhibited in Fig. 1s.

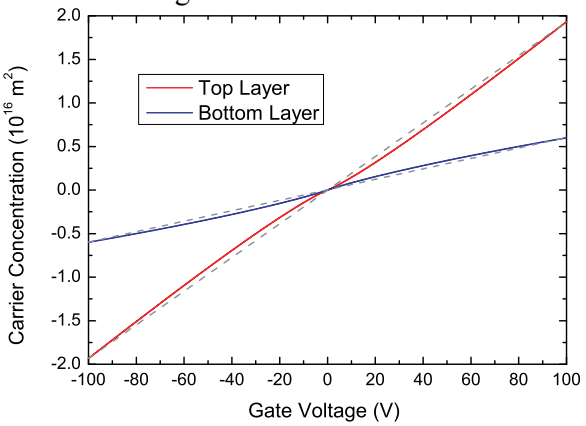

Fig 1s Carrier concentration in top (red) and bottom (blue) graphene layers of graphene/MoS_2/graphene heterostructure. Due to the screening from the bottom layer, more carriers are induced in the top layer. Gray dashed lines implies linear curves in order to verify the non-linearity of the carrier concentrations in graphene layers.

It clearly shows the non-linearity of the induced carrier concentration versus the gate voltage. Moreover, one can directly see that there always exists a difference in the carrier concentrations in top and bottom graphene layers. This difference produces different chemical potentials in each graphene layers from the relation between chemical potential and carrier concentration in graphene system; $\mu = \mathrm{sgn}(n)\hbar v_F\sqrt{\pi|n|}$. However, the whole system should be in equilibrium without bias voltage applied between two grpahene layers. Thus, Dirac cone in top graphene layer has to be shifted in order to make the chemical potentials in both layers lies at the same energy as illustrated in Fig. 2s. Since the chemical potential difference between two graphene layers gets larger as gate voltage increases, the energy shift of Dirac cone μ_0 also depends on gate voltage. Due to the Dirac cone shift, the asymmetric characteristics of tunneling current arises with respect to the direction of the applied bias voltage (see Fig. 1s).

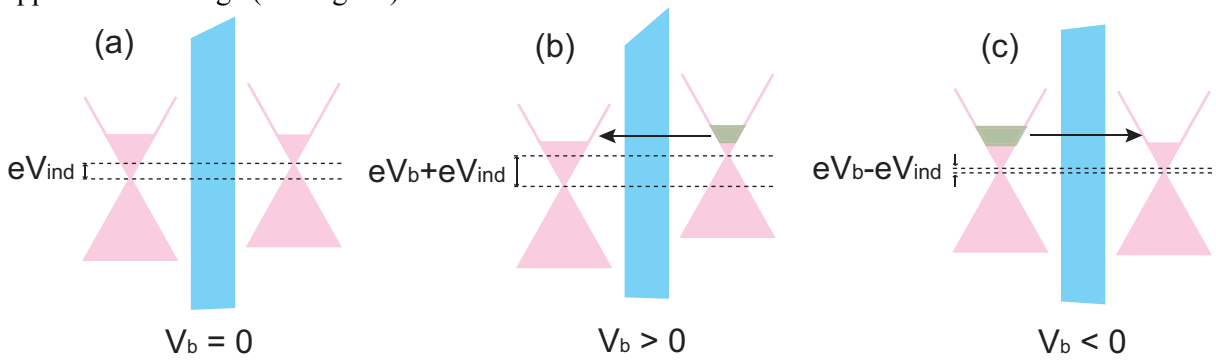

Figure 2s Energetic diagrams in each case of quantum tunneling through the heterostructures. (a) In equilibrium, the difference of chemical potentials between the top and bottom graphene layers induces a finite electric field, resulting in the shift of Dirac cone. (b) and (c) When the bias voltage is applied between two graphene layers, net tunneling current density becomes non-zero, exhibiting asymmetric characteristics due to the induced potential eV_{ind}.

3. Effects of doping MoS_2 by dopants

In the present study, an intrinsic MoS_2 layer is considered as a tunnel barrier and its Fermi level is aligned asymmetrically between the conduction and valence band edges. This asymmetry leads to the carrier-dependent feature of the tunneling current, resulting in small hole tunneling current due to the high tunnel barrier for holes. The hole tunneling current is needed to be increased because the very large spin-polarization is expected for hole tunneling through graphene/m-MoS_2/graphene heterostructures. Here, in order to increase the magnitude of the hole tunneling current, we make the MoS_2 layer doped by substitution of phosphorous atoms. Indeed, Q. Sun *et al.* theoretically showed that p-type MoS_2 is realized through substituting sulfur with phosphorous.[3]

In the intrinsic case, thermally excited carrier density is given by

$$n_i(T) = \sqrt{N_c(T)N_v(T)}e^{-E_g/2k_BT},$$

where $N_c(T) = \frac{1}{4}\left(\frac{2m_e^* k_B T}{\pi\hbar}\right)^{3/2}$, $N_v(T) = \frac{1}{4}\left(\frac{2m_h^* k_B T}{\pi\hbar}\right)^{3/2}$, and E_g is direct energy gap near K-valley of MoS_2. By defining the chemical potential in this intrinsic case, Fermi level of undoped MoS_2 is located almost at midgap, but Fermi level of MoS_2 for graphene/MoS_2 hybrid systems is asymmetrically located as aforementioned. Let us put the intrinsic Fermi level at zero energy, the valence band edge E_v = -1.4 eV.

Now, let us consider the extrinsic case. By assuming that the MoS_2 layer is neutral, the following relation between the hole density and the impurity densities is obtained by

$$p = \frac{n_i^2}{p} + N_a - N_d,$$

yielding

$$p = \frac{N_a - N_d}{2} + \sqrt{\left(\frac{N_a - N_d}{2}\right)^2 + n_i^2},$$

where N_a and N_d are acceptor and donor densities. From the carrier density, one can obtain Fermi level as below

$$E_F = E_i - k_B T \ln\left(\frac{p}{n_i}\right),$$

where $E_i = 0$. For $N_a \gg N_d$, Fermi level of p-doped MoS_2 of graphene/MoS_2 heterostructures is shown in Fig. 3s. Figure 3s shows that Fermi level of p-doped MoS2 get closer to the valence band edge as increasing dopant density. This means that one can lower the height of tunnel barrier for hole tunneling, so that the hole tunneling current can be increased by p-doping of MoS_2. Here, the valence band edge is assumed as a constant value because we consider only light doping. The larger hole tunneling current is expected for highly p-doped MoS_2 layers, but the heavy doping effects should be taken into account.

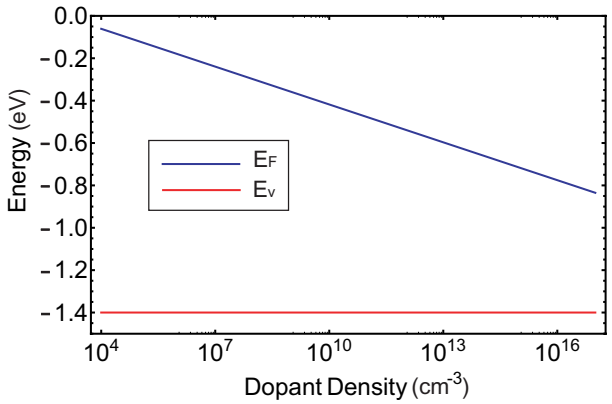

Figure 3s Log-linear plot of Fermi level of p-doped MoS2 as a function of dopant density at 300 K. Blue and red solid lines represent the Fermi level and the valence band edge of a thin MoS2 layer used in this study.

The hole tunneling current is now recalculated by considering p-doped MoS2 layers, and results are shown in Fig. 4s for different amounts of dopant density. For more dopants, larger current density is expected because the height of tunnel barrier is reduced by effects of p-doping. Of course, p-doping of MoS2 layers causes reduction in the electron tunneling current because Fermi level of p-doped MoS2 gets farther from the conduction band edge.

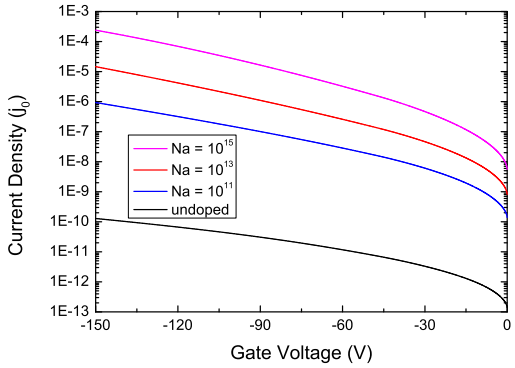

Figure 4s Hole tunneling current density as a function of gate voltage for different dopant densities of MoS_2 layers. Compared to the undoped MoS2 layer (black), current density through p-doped MoS2 layers is larger.

4. Electronic states of armchair graphene nanoribbons

The armchair graphene nanoribbons considered in this study is characterized by the number of carbon dimer lines as illustrated in Fig. 5s. By following the definition in Ref. 4, N_a-AGNR is metallic or semiconducting depending on their ribbon width. The density of states of N_a-AGNR in this study is

$$D(E) = \frac{|E|}{\pi\hbar^2 v_F^2 L_0} \sum_{n=-\infty}^{+\infty} \frac{1}{\sqrt{(E/\hbar v_F)^2 - k_n^2}},$$

where $k_n = (4\pi/3a_0)\{[3n - (N_a - 1)]/(N_a - 1)\}$ are eigenmodes of N_a-AGNR with the lattice constant of graphene a_0. Figure 6s(a) and (b) show the density of states for semiconducting and metalling AGNRs, respectively. There are van Hove singularities corresponding to the subbands of AGNRs, exhibiting the one-dimensional nature. The main difference between metallic and semiconducting AGNR is the existence of an energy gap. Here, let us note that it is not necessary to investigate both type of AGNRs because, in this study, an energy range of tunneling Dirac fermions, that we take into account (from $\mu - eV_b/2$ to $\mu + eV_b/2$) is not close to the energy gap. Thus, the calculation of the tunneling current density does not produce distinct features between metallic and semiconducting AGNRs.

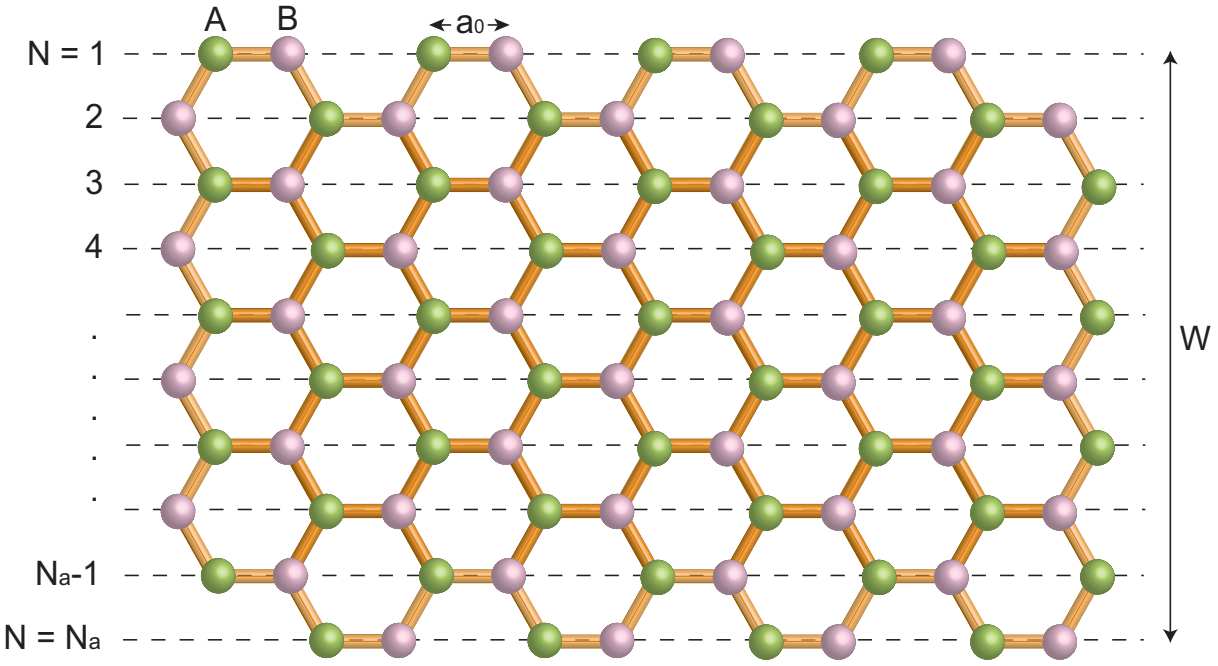

Figure 5s Schematic diagram of armchair graphene nanoribbon (AGNR). N_a is the number of carbon dimer lines (dashed lines) and W is the ribbon width of N_a-AGNR. Green and pink solid dots represent sublettices of N_a-AGNR, respectively. $a_0 \cong 1.4$ Å is the distance between adjacent carbon atoms.

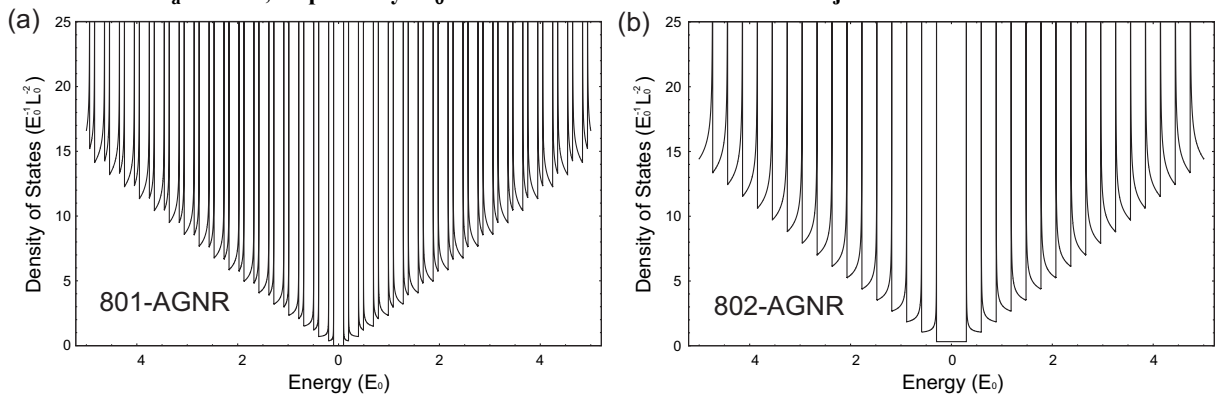

Figure 6s Density of states of (a) 801-AGNR (semiconducting) and (b) 802-ANGR (metallic). The widths of those AGNRs are (a) 98.91 nm and (b) 98.67 nm, respectively. The parameters in use are $E_0 = 141$ meV and $L_0 = 4.64$ nm.

5. Trigonal warping in graphene

Electronic structure of graphene is constructed with tight-binding approach, and the low-energy approximation allows us to have special band structures at edges of 1st Brillouin zone in k-space. These are called 'Dirac cone', leading to massless and chiral characters of quasi-particles, so-called Dirac fermions. In the low-energy approximation, Dirac fermions are governed by Dirac fermions instead of Schrödinger equation. The energy dispersion of Dirac fermions is solved as

$$\varepsilon_k = \frac{3a_0 t}{2}\sqrt{k_x^2 + k_y^2},$$

which is isotropic near K-valleys.

On the other hand, we cannot neglect high-order terms when energy is not sufficiently small. In this case, energy dispersion relation is different from the low-energy

approximation as below (Ref. 5)

$$\varepsilon_k = \frac{3a_0 t}{2}\sqrt{\left(k_x^2 + k_y^2\right) + \frac{a_0^2}{16}\left(k_x^4 + k_y^4\right) + \frac{a_0}{2}\xi\left(k_x^3 - 3k_x k_y\right)},$$

where $\xi=\pm1$ represent different K-valleys. The resulting dispersion is anisotropic and nonequivalent for each valley. The energy range for this case is about several 100 meV, so that it is not negligible in practice.

Figure 7s shows band structure of grpahene in k-space including only nearest neighbor hoppings. One can easily see that there are six points where the conduction and the valence bands tough each other, resulting in a zero band gap. At low-energy, we can see that Fermi surface is circular and equivalent near Dirac points. However, at higher energy (not too high), Fermi surface is round triangular and nonequivalent for each valley. Due to the shape of Fermi surface, this effect is named 'Trigonal warping'.

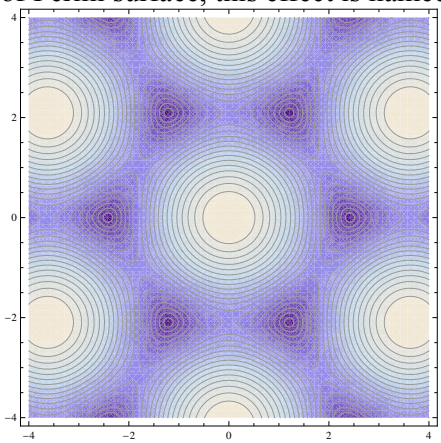

Figure 7s Contour plot of energy bands of graphene. Bright and dark colors correspond to high and low energy. Six darks points are six Dirac points with zero energy. Away from Dirac points, contour lines become triangular. The trigonal warping is valid for this energy range.

In the present study, the energy range of tunneling Dirac fermions is also several 100 meV. For example, chemical potential of the bottom graphene layer is ~282 meV for V_g = 150 V. Therefore, in our case, effects of the trigonal warping can be considered. As a consequence of the trigonal warping, in-plane current through graphene layers can be valley-polarized.

Note that the tunneling current through the spin-split direct gap dear K(K')-valley of MoS2 is spin-up(down)-polarized. This means that we can obtain spin-up(down)-polarized current if we have K(K')-valley-polarization. Indeed, a valley-filter, which produces fully valley-polarized electron beams, has been proposed by J. L. Garcia-Pomar et al.[6] The valley-filter is set at the end of one graphene electrode, separated from the tunneling region as shown in Fig. 8s.

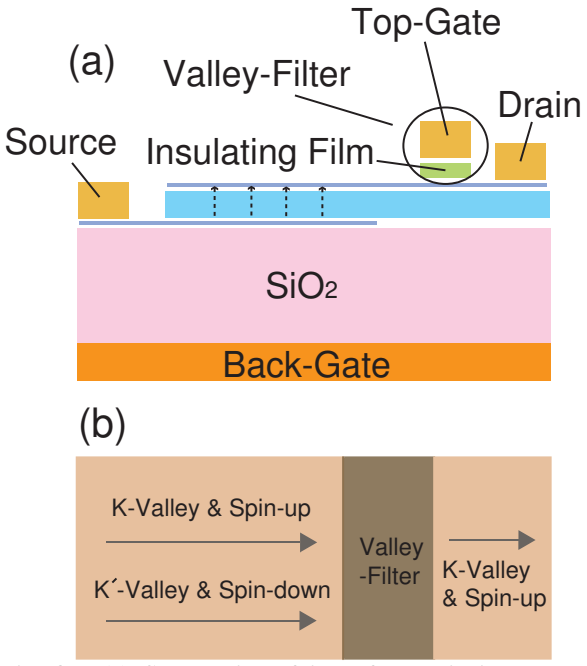

Fig. 8s (a) Schematics of idea for achieving non-zero spin-polarization. The valley-filter should be separated from the tunneling region because the top-gate may affects on vertical tunneling. (b) Spin-polarized current can be achieved by the valley-filter because most of the spin-up(down) Dirac fermions near K(K')-valley.

Finally, we can conclude that it is possible to achieve the spin-polarized tunneling current through the graphene heterostructure in practice, taking into account the trigonal warping.

REFERENCES

(1) Yu, W. J.; Li, Z.; Zhou, H.; Chen, Y.; Wang, Y.; Huang, Y.; Duan, X. Vertically Stacked Multi-Heterostructures of Layered Materials for Logic Transistors and Complementary Inverters. *Nat. Mater.* **2013**, 12, 246-252.

(2) Britnell, L.; Gorbachev, R. V.; Jalil, R.; Belle, B. D.; Schedin, F.; Mischenko, A.; Georgiou, T.; Katsnelson, M. I.; Eaves, L.; Morozov, S. V. *et al.* Field-Effect Tunneling Transistors Based on Vertical Graphene Heterostructures. *Science* **2012**, 335, 947-950.

(3) Sun, Q.; Li, Y.; He, J.; Yang, W.; Zhou, P.; Lu, H.; Ding, S.; Zhang, D. W. The Physics and Backward Diode Behavior of Heavily Doped Single Layer MoS_2 Based p-n Junctions. *Appl. Phys. Lett.* **2013**, 102, 093104.

(4) Myoung, N.; Ihm, G.; Lee, S. J. Transport in Armchair Graphene Nanoribbons Modulated by Magnetic Barriers. *Physica E.* **2010**, 42, 2808-2811.

(5) Pereira Jr. J. M.; Peeters, F. M.; Costa Filho, R. N.; Farias, G. A. Valley Polarization due to Trigonal Warping on Tunneling Electrons in Graphene, *J. Phys.: Condens. Matter* **2009**, 21, 042301.

(6) Garcia-Pomar, J. L.; Cortijo, A.; Nieto-Vesperinas, M. Fully Valley-Polarized Electron Beams in Graphene, *Phys. Rev. Lett.* **2008**, 100, 236801.